A&A 423, 833–847 (2004)
DOI: 10.1051/0004-6361:20035637

Astronomy & Astrophysics

Peculiarities and populations in elliptical galaxies

I. An old question revisited⋆,⋆⋆,⋆⋆⋆

R. Michard[1] and P. Prugniel[2]

[1] Observatoire de Paris, LERMA, 77 Av. Denfert-Rochereau, 75015 Paris, France
e-mail: raymond.michard@obspm.fr
[2] Centre de Recherches Astronomiques, Univ. Lyon 1, Observatoire de Lyon, 69561 St. Genis Laval Cedex, France

Received 6 November 2003 / Accepted 26 March 2004

Abstract. Morphological peculiarities, as defined from isophote asymmetries and number of detected shells, jets or similar features, have been estimated in a sample of 117 E classified galaxies, and qualified by an ad hoc Σ_2 index. The overall frequency of "peculiar" objects (*Pec* subsample) is 32.5%. It decreases with the cosmic density of the environment, being minimal for the Virgo cluster, the densest environment in the sampled volume. This environmental effect is stronger for galaxies with relatively large Σ_2.
The *Pec* subsample objects are compared with "normal" objects (*Nop* subsample) as regards their basic properties. Firstly, they systematically deviate from the Fundamental Plane and the Faber-Jackson relation derived for the *Nop* subsample, being too bright for their mass. Secondly, the dust content of galaxies, as estimated from IRAS fluxes, are similar in both subsamples. Third, the same is true of the frequency of Kinematically Distinct cores (KDC), suggesting that KDC and morphological peculiarities do not result from the same events in the history of E-galaxies.
Using the *Nop* sample alone, we obtain very tight reference relations between stellar population indicators ($U-B$, $B-V$, $B-R$, $V-I$, Mg_2, Hβ, $\langle\mathrm{Fe}\rangle$, Mg$b$) and the central velocity dispersion σ_0. The discussion of the residuals of these relations allows us to classify the *Pec* galaxies in two families i.e. the *YP* or NGC 2865 family, and the *NP* or NGC 3923 one. Galaxies in the first group show consistent evidence for a younger stellar population mixed with the old one, in agreement with classical results (Schweizer et al. 1990; Schweizer & Seitzer 1992). The second group, however, has "normal", or reddish, populations. It is remarkable that a fraction (circa 40%) of morphologically perturbed objects do not display any signature of a young population, either because the event responsible for the pecularity is too ancient, or because it did not produce significant star formation (or eventually that the young sub-population has high metallicity).
A preliminary attempt is made to interpret the populations of *Pec* objects by combining a young Single Stellar Population with a *Nop* galaxy, with only limited success, perhaps largely due to uncertainties in the SSP indices used.

Key words. galaxies: elliptical and lenticulars, CD – galaxies: photometry

1. Introduction

Although peculiar galaxies were systematically studied by Arp (1966), Malin (1979) was possibly the first to describe "shells" and "jets" in the otherwise rather normal E-type galaxy M 89 (NGC 4552). From their catalogue of southern *shell galaxies*, Malin & Carter (1983) (MC83) found that such features occur in about 17% of ellipticals, mostly field objects, the percentage being drastically reduced among cluster galaxies. A special effort was also devoted to measuring the photometric properties of shells (Fort et al. 1986), and to get extensive spectral information (Carter et al. 1988).

On the theoretical side, since very peculiar objects (sometimes barely fitting in the Hubble classification!) could be convincingly identified with *ongoing mergers* or recent merger remnants (Toomre & Toomre 1972), it was proposed (Toomre 1977; Barnes 1988) that all E galaxies were the result of the mergers of disk galaxies. Also the interactions of a large E with smaller satellites were modeled to explain the relatively modest peculiarities in part of E-S0 galaxies, such as "shells" or "ripples", "jets", "plumes", boxy isophotes, not to speak of "X-structures". We refer to the review by Barnes & Hernquist (1992) for a description of this early work.

In the late eighties, Schweizer and coworkers studied the correlations between an ad hoc "peculiarity index" Σ of E galaxies and their stellar populations, as characterized by line

⋆ Based in part on observations collected at the Observatoire de Haute-Provence.
⋆⋆ Figures 1–3 are only available in electronic form at http://www.edpsciences.org
⋆⋆⋆ Table 10 is only available in electronic form at the CDS via anonymous ftp to cdsarc.u-strasbg.fr (130.79.128.5) or via http://cdsweb.u-strasbg.fr/cgi-bin/qcat?J/A+A/423/833

indices (Schweizer et al. 1990) or *UBV* colours (Schweizer & Seitzer 1992) (SS92). This was extended to S0s in Schweizer & Seitzer (1988), and also in the quoted papers. Unfortunately the observational basis of this work was never published in detail. On the other hand the sample of Es studied was rather small and strongly biased, with cluster galaxies nearly absent. Finally, the "good correlations" found by Schweizer and coworkers between their Σ peculiarity index and galaxy populations, are rather surprising, because they would imply that interactions always produce young stars as well as morphological deviances. This does not seem likely in E+E or E+S0 encounters, where both the intruder and the target are quite poor in interstellar matter. Also the time scale for the morphological features to relax toward a symetrical equilibrium status is often longer than the stellar evolution time scale after which the burst becomes undiscernable over the underlying old population.

Our purpose in the present work is to reconsider the relations between morphological "peculiarities" and population changes in E-type galaxies: such relations are indeed quite likely, but, in view of the large variety of possible interactions, there is no reason why they should be simple and straightforward. The cosmic environment is probably important in defining the frequencies of encounters and the character of the participants. We tried to make some progress in a complex problem by using a relatively large sample of 117 objects, and also a statistically complete one (or nearly so), in the Local Supercluster. Again a peculiarity index Σ_2 has been defined, to be compared with other galaxy parameters. In contrast to the Σ in SS92, the new index relies, almost exclusively, upon measurable parameters in the images of the studied galaxies.

In Sect. 2 our techniques of morphological analysis are described, and the elements concurring to the formation of Σ_2 are defined. Basic properties of "peculiar" and "normal" ellipticals are intercompared in Sect. 3, including the frequencies of peculiar Es depending upon the local density of galaxies: the sample is still unsufficient however, to consider this problem in satisfactory detail. In Sect. 4 possible correlations between the presence of peculiarities and the stellar populations, as described by colours and line indices, are considered. In the discussion (Sect. 5) we argue that no straightforward correlations are expected between the morphological traces and the population changes left by an interaction. The game of interactions between galaxies is a complex one and much effort will be needed to learn its rules.

2. Sample and data

2.1. The sample

Most of our sample has been extracted from the catalogue of early-type galaxies built by Prugniel & Simien (1996) for a study of the Fundamental Plane (PS96). Objects with a distance modulus larger than 33.52 and absolute B magnitude $M_t(B)$ fainter than −18.8 have been discarded, both parameters being taken from PS96. E-types have been checked from the RC3. A few objects with regions of recent star formation have been rejected, i.e. NGC 3156 (Michard 1999), and also objects with large galactic extinction. Several galaxies not listed in PS96 have been added, especially to increase the subsample from the Centaurus Group.

For nearly all the 117 objects in the sample, we have the B_t^0 magnitude from PS96, their distance moduli from a model of the Local Supercluster velocity field, their adopted effective surface brightness $\mu_e(B)$ and corresponding radius r_e, their adopted central velocity dispersions σ_0 and rotation velocities. We have reconsidered the colour system for the sample galaxies: Poulain & Nieto (1994) give the four colours $U-B$, $B-V$, $V-R$ and $V-I$ from relatively homogeneous observations for most galaxies in our sample; these were corrected for galactic extinction and K-effects according to the RC3 precepts. If not available, they were completed by the PS96 *UBV* colours or by the *VRI* colours from Prugniel & Héraudeau (1998).

Other data of interest are:

- *the SBF distances* (based on Surface Brightness Fluctuations) by Tonry et al. (2001): these are available for 92 objects in the sample (only 89 finally kept as genuine Es), and are used below in parallel with the PS96 distances. *These two sets of distances correlate quite well.* If X is the SBF distance modulus and Y the PS96 value, the impartial correlation for the studied sample is $Y = 0.958 \pm .053 \cdot X + 1.13 \pm .04$ with a coefficient of correlation of 0.85 and $\sigma = 0.37$;
- *the line population indices* Mg_2, Hβ, ⟨Fe⟩, Mgb: the first has been taken from the HYPERLEDA data base, maintained by the Centre de Recherches Astronomiques de Lyon. The others were derived from a compilation of data in Trager et al. (1998), i.e. the Lick/IDS observations which provide most of the available data; Trager et al. (2000); Kuntschner (2000); Kuntschner et al. (2001); Bueing et al. (2002). Before averaging, these data sets were tentatively brought into a common scale by adding ad hoc small constants. For Hβ, individual values possibly affected by emission were rejected, in practice indices smaller than 1 Å;
- *the local cosmic density* was specially calculated for the surroundings of our objects, following Prugniel et al. (1999) but with improved redshift data. This is measured from adequate automatic groupings of galaxies in 3D, and normalized to the Virgo cluster;
- *morphological information*, such as the ellipticities at r_e, was obtained from surveys by Goudfrooij et al. (1994), Michard & Marchal (1994). The classification in terms of *disky, boxy, undeterminate* ellipticals (or *di*E, *bo*E, *un*E respectively) was derived from data in the same surveys, and/or from Caon et al. (1994). The frames collected for the present work, and their analysis described below, were also usable for this purpose, but the DSS frames are sometimes not favourable for detecting the faint inner disks of *di*Es, due to photographic saturation.

2.2. The used frames and their treatment

2.2.1. The frames

Two series of frames have been used for studying peculiarities, if any, in the sample galaxies.

– The Digital Sky Survey (DSS) quite easily provides convenient frames for our purpose. We have used only the *B* and *R* surveys, providing 2 frames from the UK Schmidt Telescope for the southern hemisphere, and generally 3 frames from the Palomar Schmidt for the northern. A precious property of the DSS frames is the free choice of the collected field: we have used fields of 10′ or 17′ square for most objects, and up to 28′ for a few large Virgo cluster galaxies.
  As shown below, the "depth" and resolution of these frames are adequate to detect faint outer shells and jets in galaxy pictures. The sharpness of stellar images, not surrounded by excessive scattered light in extended wings, is a useful feature in crowded fiels. On the other hand, the images of giant Es are saturated in a range of radii which may extend to r_e: this precludes the detection of inner ripples or any other structure close to the center.
– Deep CCD frames in 5 colours have been collected for 36 Es of the present sample by Idiart et al. (2002) (IMP02). They were obtained at the 120 cm telescope of the OHP (Observatoire de Haute Provence) with an angular field of nearly 12′ square. These were supplemented by frames available from the HYPERLEDA database, taken with the same CCD, or in a few cases with a smaller one offering a field of only 7′ square. The OHP pictures suffer from a rather poor seeing, i.e. 2−3 arcsec *FWHM* for the frames used in the present study. The stellar images are affected by extended wings (see Michard 2002), which may be troublesome when superimposed upon a galaxy picture.

2.2.2. The treatment: Preparations

1. *Averaging of frames*. Whether using the DSS or the OHP frames, we tried to increase the S/N ratio, and still more *to lessen residual background fluctuations*, by averaging two or three frames, that is the three *BVR* frames for the CCD material, the two or three available frames for the DSS. Appropriate weights were introduced in averaging, to minimize the residual sky background variations, against possibly different photometric scales of different frames. Average frames were conventionally considered as "white" frames. It has been verified that a "white" frame, so derived from 3 *BVR* frames, is quite similar to a *V* frame, at least for E galaxies with their small colour gradients. Accordingly, we calibrated our CCD "white", or *W* frames, with the available *V* photometry: this approximation is adequate for the purposes of this paper. When useful, the outer parts of *W* frames from the DSS material were calibrated by comparison with the photometry by Michard (1985), Caon (1994), or IMP02.
2. *Sky background*. Large-scale background fluctuations are a nuisance in the photometry or even the morphology of galaxies at low residual surface brightness. Malin averages several deep Schmidt frames to bring out the faint outermost structure apparently surrounding a number of large E-S0 objects (see Malin & Hadley 1999). In IMP02, background fluctuations surviving the flat field routine could be reduced to 0.2−0.4%, depending on colour, by a careful "mapping" of the "sky" far from the studied object. Such a procedure was also found necessary for the DSS frames. For instance the outer parts of M 87 at light levels less than $V = 24$ look very different in the three available frames of field 28′: the galaxy is asymmetric, with northward brightening for two of these, and southward brightening for the third. Such trends are probably due to variations in the photographic fog: they are easily mapped and corrected for, but over- or undercorrection are always possible, leaving errors in the isophotal contours. For the quoted example of M 87, the averaging of 3 DSS frames, followed by fitting a flat sky (linear in x, y) cancels out the asymmetries seen in individual frames: the isophotal contour at $V = 26$, or about 1% of the sky level, is nearly symmetric,but the only way to check this would be to study other deep, large field, frames.
3. *Isophotal analysis*. Our *W* frames were analyzed according to Carter (1978) (see Michard & Marchal 1994, for details). The output of this routine is a table of isophotal contours, containing for each isophote the 5 parameters of the best-fitting ellipse, the harmonic coefficients of deviations to this ellipse, and a quantity related to the surface brightness. The 4th cosine harmonic, termed a_4 in Bender & Möllenhof (1987), or e_4 in Michard & Marchal (1994) is a measure of disky or boxyness. In the present work, the isophotal analysis was used to find the ellipticity at r_e and to locate the object among the 3 subclasses *di*E, *bo*E or *un*E. In a few cases, due to the saturation of the DSS frames, the well-known correlation between isophotal forms and kinematics (Bender 1988) was used to check the classification.
  Remark: the isophotal analysis is applied to an auxiliary frame, previously cleaned of parasitic objects (see IMP02). This exercise becomes rather tedious in wide and crowded fields, and one should keep in mind that it does not truly restore the corrupted galaxy picture.
4. *Masking*. "Unsharp masks" from photographic techniques have been successfully applied in MC83 to display inner shells in several objects such as NGC 3923. The calculation of such masks is also discussed by Prieur (1988). SS92 mention masking "with various derivative images obtained by convolution with $\sigma = 5''$ and $10''$ Gaussians". We were disappointed by our tests of this simple approach, and adopted instead "synthetic masks", calculated from the previously-obtained isophotal analysis. Using the complete file of parameters resulting from this operation, one may synthesize an image closely resembling the input galaxy image. One may however modify the table of parameters to produce a "mask" with specific properties:
   – if the *center coordinates* are kept constant, the mask reveals large-scale asymmetries of the original galaxy image;
   – if *odd harmonics* are put to zero, the mask has a center of symmetry (provided of course that the first above condition is kept). The faint dust patterns of E-galaxies, or any non-symmetrical features, are emphasized;
   – if *even harmonics* are put to zero, the mask emphasizes the diskyness or boxyness of the contours. If all harmonics are put to zero, the mask has elliptical

isophotes: its effects upon the image may be sometimes misleading;
- if the *orientation* is kept constant, the mask strongly emphasizes the isophotal "twists". This may help to detect incipient bar structures.

Changes of the isophotal axis ratio should be avoided, except for some smoothing of noise-induced fluctuations.

In the present work, *we have used masks fulfilling both the first and second properties above. They have the same resolution as the input images. Division by such a mask emphasizes non-symmetrical features*. Actually we have applied the relation $(MaskedImage) = (InputImage)/(Mask)^{0.9}$, the power below 1 being intended to preserve part of the original image gradient. Since the isophotal analysis of the frame does not reach much below a surface brightness level of about $V = 25$, the mask has to be extended at large r values, outside the radial calculated range. Two techniques have been used for this purpose: a polynomial extrapolation of the measured light-radius relation, or the actual extension of the measurements of the residual light at large r along assumed elliptical contours. With this second technique, the mask does not extend to the very edge of the frame, as may be seen in part of Figs. 1 and 2.

2.3. "Normal" ellipticals and peculiarities

2.3.1. "Normal" ellipticals

A *normal E-type galaxy* is defined here as having centrally symmetric and nearly elliptical isophotes. Accordingly, the so-called twist of isophotes, their eventual disky- or boxyness are not considered as peculiarities: the various sub-types, *di*E (disky E), *bo*E (boxy E) or *un*E (undeterminate) are not a priori distinguished in this study. This calls for some discussion however. In SS92, boxyness is considered as a trace of interaction of the E-type object with some intruder, following calculations by Hernquist & Quinn (1989). These are however challenged by Lima-Neto & Combes (1995) who find that "dissipationless mergers tend to wash out any disky or boxy isophotes instead of creating them". Various authors (Michard 1994; Scorza & Bender 1995; Kormendy & Bender 1996; Scorza et al. 1998) have emphasized the similarities of *di*Es to S0s on morphological and kinematical grounds. It remains true however, as will be further checked below, that the various sub-types of ellipticals remain closely alike as regards such basic properties as the $r^{1/4}$ law, the Faber-Jackson relation, the Fundamental Plane, the colours and line-indices of their stellar populations. We feel justified therefore in treating the problem of peculiarities for the three sub-types together.

2.3.2. A peculiarity index

As in SS92 we have defined a *peculiarity index* Σ_2 from several elements.

- *Discrete features* classically recognized in possible post-mergers or in perturbed E-galaxies are "shells", at the "edge" of the object or eventually far out. They may be seen on direct images as in MC83 (Examples: NGC 4552, Fig. 3). Inner shells, or "ripples" as termed by Schweizer & Ford (1984), are better seen in masked images. They may form complex systems with evidence of regularities (example: NGC 3923, Fig. 2; see also Prieur 1988). Various outwards extensions may be seen in both masked or unmasked images, termed "jets" if nearly straight or "fans" if curved (examples: NGC 4552 for a jet; NGC 1549, Fig. 2 for both forms). We have estimated the number nF of all kinds of such discrete features. This number obviously depends on the S/N ratio of the available pictures, and eventually of their field. It has been checked that the two sources of material used here essentially give the same nF for a given object, but dedicated studies could possibly detect, in some cases, more low-contrast features.
- *E-classified galaxies* retain the canonical elliptical form in their central regions, but discrete peculiar features are currently associated with a general asymmetry of the outer regions (IC 3370, Fig. 3 is a rather extreme example). Such asymmetries may also occur without discrete peculiarities: the isophotes remain grossly elliptical, but their centers drift away from the core of the object. A good example is NGC 5846 (Fig. 1). This or similar phenomena have been described and modelized by Combes et al. (1995).

  We have derived an index for such asymmetries by selecting, in an isophotal map, a fiducial diameter of apparently maximal asymmetry, estimated the radial range $\Delta(r/r_e)$ where the asymmetry is detected (expressed in terms of the effective radius r_e), and measured on several intervening isophotes the ratio r_M/r_m of the larger to the minor radius. A mean amplitude $mA = 10(\langle r_M/r_m \rangle - 1)$ is readily obtained. Then the asymmetry index is defined as $cA = mA \cdot \Delta(r/r_e)$, i.e. the product of the observed range by the mean asymmetry. This figure varies between 0 (no convincing asymmetry) to about 7. There is a general correlation between the two indices nF and cA. There is however a fair proportion (about 1/3) of objects with asymmetries but without discrete peculiar features.
- *Perturbed envelopes* are defined as apparently anomalous forms of the envelopes without large departures from the central symmetry. This might be the case of the X-pattern displayed by Arp230 (see Schweizer & Ford 1984). Such cases seem rare, but led us to add an increment $dA = 0.5$ to the measured asymmetry index of three galaxies. In other cases $dA = 0$.
- *Our final peculiarity index* is $\Sigma_2 = cA + dA + nF^{1/2}$. It varies from 0 to slightly above 10 for NGC 2865 and 3923, the most peculiar objects in our sample.

  This index is affected by various sources of uncertainties. The overall correctness of the cA term has been checked by measuring asymmetries for 9 large galaxies, both from OHP and DSS frames: its values never differ by more than 1. For many other objects however, the crowding of stars in the field, or the presence of large parasitic objects, such as bright stars or nearby galaxies, impair the location of isophotes and prevent reliable estimates of their asymmetries. The nF term will be often lessened, i.e. features will be missed, by poor resolution, partial saturation

or low S/N in DSS frames... but it enters only through its square-root in the final index Σ_2. The distribution of errors in Σ_2 is certainly far from normal, and cannot be described by a standard deviation. A relative error of 25% is probably a conservative upper limit.

3. Observational results: morphology

3.1. The morphological data

The data from the present work is presented as follows:

- A complete table (Table 10) is to be published in electronic form through the CDS Strasbourg. It contains, for all the sample, the literature data used to study the correlations between the morphology and other galaxy properties, plus our morphological results, sub-types and ad hoc indices Σ_2 and MIYP (see definition in Sect. 4.4). From the 117 objects in the sample, we have rejected 3, which are perhaps not genuine ellipticals: NGC 1209 is probably an SB0/a, while NGC 6851 and 6909 are tentatively classified SAa.
- Table 1 gives the list of the 37 galaxies detected as "peculiar". For the sake of brevity the members of this list will be called the *Pec* subsample. Two objects with a measured index $\Sigma_2 < 1$ have been reclassified as "normal". We thus have 77 galaxies without detected morphological peculiarity, and forming the *Nop* subsample.
  This table contains the adopted sub-types; two parameters giving an indication of the radial range actually analyzed for each object, i.e. the limiting measured isophote $R_{\max}$ in terms of the effective radius, and eventually the corresponding V surface brightness; the final Σ_2 index and the three components of its evaluation (see Sect. 2.3.2) *cA* (for asymmetry), *nF* (for features) and the additive correction *dA* (generally zero).
- Displays of 18 objects are given in Figs. 1–3, available only in the electronic version of the paper. Figure 1 contains both direct and masked pictures for 6 galaxies studied from OHP CCD frames. The displays for NGC 3377 are derived from the composite of 6 deep frames: they do not reveal shells or ripples, contrary to the index Σ of SS92 implying the detection of 2 such features. NGC 5846 is the best example of a galaxy with large asymmetry but no other features of peculiarity. The other are characteristic cases of peculiar objects with both asymmetry and ripples, these best seen in masked frames.
  Figure 2 contains a similar presentation of 6 objects from the DSS material. Again we have introduced for comparison an apparently normal object, NGC 4636, with negligible asymmetry. The others, i.e. NGC 1344, 1549, 2865, 3923 and 5018 are classical examples of strongly peculiar objects with important systems of shells and/or outwards extensions.
  Figure 3 displays the direct images of 6 objects (NGC 1700 is from OHP frames, the others from the DSS). Of interest are the 3 galaxies, NGC 1700, 4125 and 4406, where the asymmetry index was increased by $dA = 0.5$ to take into account the perturbed envelope. The remarkable features of NGC 1395, 4552 and IC 3370 are easily seen from the direct images.
- Individual notes for illustrated objects, in order of increasing morphological peculiarities.
  NGC 3377 (Fig. 1): no detected asymmetry.
  NGC 4636 (Fig. 2): no detected asymmetry.

Table 1. Detected peculiarities in the *Pec* subsample of ellipticals. (1) Name; (2) sub-type; (3) $R_{\rm m}$ radius of the outermost measured isophote in terms of the effective radius; (4) the corresponding surface brightness $V_{\rm m}$ if measured; (5) *cA*, asymmetry index measured as explained in text; (6) *nF*, number of detected features; (7) additive constant for peculiar outer isophotes of modest asymmetry; (8) final Σ_2 index as defined in text.

Name	Sty	$R_{\rm m}$	$V_{\rm m}$	*cA*	*nF*	*dA*	Σ_2
NGC 0596	*di*E	4.2	–	1.1	1	0	2.1
NGC 1344	*di*E	4.2	–	3.2	5	0	5.5
NGC 1395	*un*E	4.8	–	2.8	1	0	3.8
NGC 1399	*un*E	4.6	–	2.0	0	0	2.0
NGC 1537	*di*E	5.5	–	1.2	1	0	2.2
NGC 1549	*bo*E	6.5	–	4.6	6	0	7.0
NGC 1653	*un*E	4.1	–	3.6	0	0	3.6
NGC 1700	*di*E	5.4	25.0	3.3	0	0.5	3.8
NGC 2768	*di*E	3.9	25.6	1.2	0	0	1.2
NGC 2865	*un*E	4.5	–	8.0	7	0	10.6
NGC 2974	*di*E	7.1	–	2.2	2	0	3.6
NGC 3557	*un*E	5.1	–	3.3	1	0	4.3
NGC 3585	*di*E	6.8	–	1.8	1	0	2.8
NGC 3610	*di*E	8.2	26.0	4.8	4	0	6.8
NGC 3613	*di*E	6.2	26.0	0.7	1	0	1.7
NGC 3640	*bo*E	5.6	25.5	6.8	4	0	8.8
NGC 3923	*un*E	6.0	–	7.3	9	0	10.3
NGC 4125	*di*E	4.8	25.5	2.0	0	0.5	2.5
NGC 4374	*bo*E	3.8	26.3	2.1	0	0	2.1
NGC 4406	*bo*E	3.4	25.0	2.6	0	0.5	3.1
IC 3370	*bo*E	3.8	–	6.0	3	0	7.7
NGC 4552	*un*E	6.4	26.3	2.2	3	0	3.6
NGC 4767	*bo*E	5.6	–	3.3	0	0	3.3
NGC 4976	*un*E	5.5	–	3.0	5	0	5.2
NGC 5018	*di*E	5.9	–	5.6	6	0	8.0
NGC 5061	*bo*E	6.0	–	3.2	0	0	3.2
NGC 5077	*un*E	5.2	–	4.8	0	0	4.8
NGC 5322	*bo*E	5.0	–	2.6	0	0	2.6
NGC 5557	*un*E	5.1	–	5.3	2	0	6.7
NGC 5576	*bo*E	6.2	26.0	6.6	2	0	8.0
NGC 5846	*un*E	4.0	26.4	4.7	0	0	4.7
NGC 5982	*bo*E	6.9	26.0	5.8	1	0	6.8
NGC 6411	*un*E	3.7	–	1.6	2	0	3.0
NGC 7454	*di*E	4.1	–	2.5	0	0	2.5
NGC 7507	*un*E	6.8	–	3.6	1	0	4.6
NGC 7619	*un*E	3.8	–	1.8	1	0	2.8
NGC 7626	*un*E	3.2	–	–	2	0	1.4

NGC 4406 (Fig. 3): no features, faint asymmetry and "bean-like" outer isophotal contours (one side convex, the other concave).
NGC 4125 (Fig. 3): no features, faint asymmetry and cross-like outer isophotal contours.
NGC 1700 (Fig. 3): no features, faint asymmetry and X-like outer isophotal contours.
NGC 1395 (Fig. 3): faint asymmetry, one sharp shell.
NGC 5846 (Fig. 1): no features, but large general asymmetry towards NE, readily seen and measured in both OHP and DSS images. Is an interaction with the compact NGC 5846A responsible, or with the giant spiral 5850 (see Higdon et al. 1998)?
NGC 4552 (Fig. 3): faint asymmetry, bright jet SE, sharp shell S and diffuse feature NNE.
NGC 5982 (Fig. 1): strong NS asymmetry, faint diffuse feature.
NGC 3610 (Fig. 1): moderate asymmetry, one sharp and several diffuse features.
NGC 3640 (Fig. 1): strong asymmetry, several sharp and diffuse features (see discussion in Prugniel et al. 1988; also compare with NGC 6776, not in the present sample but studied by Sansom et al. 1988).
NGC 5576 (Fig. 1): very strong asymmetry, important features.
IC 3370 (Fig. 3): extreme asymmetry, several features, square isophotes (nearly X-like as in tumbling bars).
NGC 1344 (Fig. 2): moderate asymmetry, important shell system.
NGC 1549 (Fig. 2): asymmetry, numerous shells and outer jets.
NGC 5018 (Fig. 2): strong asymmetry, several inner and outer features
NGC 3923 (Fig. 2): asymmetry, very rich system of shells.
NGC 2865 (Fig. 2): strong asymmetry, bright shells and complex system of ejecta.

3.2. Comparison with previous results

As might be expected, the images collected here are in agreement with published pictures in MC83 for NGC 1344, 1549, 2865, 4552, provided the field or S/N ratio were comparable. Shell galaxies in the MC83 catalogue are seen as peculiar, if members of the present sample, except an exception: MC83 indicate a "shell to the NW" in NGC 7145. We considered this feature as doubtful and discarded the object from Table 1. It may be noted that the extremely faint extended features described by Malin and coworkers around a number of large galaxies (see recapitulation in Malin & Hadley 1999) are generally not detected from the here available material. For instance, NGC 4486 is a "normal" giant elliptical by our criteria, altough Malin detects asymmetric extensions at a very low surface brightness. Its classification is usually ended by the letter *p* in most catalogues, due to the famous inner jet.

The comparison between our peculiarity indices Σ_2 and the similar Σ listed in SS92 is disappointing. The results are statistically incompatible: we find 67% of ellipticals to be normal, with $\Sigma_2 \leq 1$, while in SS92, out of 34 Es (NGC 3156 rejected), only 10 (or 29%) have $\Sigma \leq 1$. One reason of the discrepancy lies in selection effects of the SS92 sample, biased in favor of small groups and against the Virgo cluster. For 30 objects in common, the Σ indices are compatible only in 15 cases. It appears that a number of SS92 objects are listed with Σ values implying a number of detected ripples which we do not see, even when our material is exceptionaly good, as noted above in the case of NGC 3377. On the other hand, we list 2 ripples in NGC 2974, an object with $\Sigma = 0$ in SS92.

Table 2. Occurence of peculiar Es against the local cosmic density D of galaxies. ΔD range of D; *structures* Corresponding structures; N total number of objects; $n1$ number of objects with $\Sigma_2 < 3$; $n2$ number of objects with intermediate Σ_2, i.e. 3 to 5; $n3$ number of objects with $\Sigma_2 > 5$.

ΔD	*Structures*	N	$n1$	$n2$	$n3$
$D < 0.21$	Very poor groups	58	7	5	7
$0.21 < D < 0.41$	Poor groups	23	2	4	3
$0.41 < D < 0.61$	Fornax, N1600	8	1	0	1
$0.61 < D < 0.81$	ComaI, Pegasus	4	2	0	0
$D > 0.9$	Virgo, Centaurus	21	2	2	1
$D \sim 1$	Virgo alone	16	2	1	0

3.3. Statistics of the occurrence of "peculiar" Es

According to our criteria, there are 32.5% of "peculiar" ellipticals. Among the 37 objects in the *Pec* subsample, 24 have shells, jets or other discrete features; the remaining 13 only display some asymmetry of the NGC 5846 kind, and have often a small Σ_2 index. If we consider only these objects with $nF > 0$, the proportion of peculiars decreases to 22% and becomes quite compatible with inferences in MC83 for the proportion of shell galaxies among ellipticals. As suggested in the same paper, the proportion changes with the environment of the E object, being minimal for clusters and maximal for field objects.

The question is considered quantitatively in Table 2, where the sample is sorted out into various categories of environments, characterized by the local density D: this quantity is 1 for the Virgo Cluster. The distribution of our sample is quite inhomogeneous in terms of D, with about half of the objects in rather small and loose groups with $D < 0.21$, and 71% with $D < 0.41$. Our statistics are therefore uncertain, each category of cosmic density being represented by too small numbers. It appears however that the most peculiar objects, i.e. with $\Sigma_2 > 5$ form 12% of the subsample of small D ($D < 0.41$) but 6% of the galaxies in denser groups, the Virgo cluster and extensions containing no such extreme object. We find only 3 peculiar objects among the 16 Es here observed in Virgo and extensions, that is about half the general proportion of 1/3. Considering the objects with $\Sigma_2 > 3$, only one, i.e. M 89, is found in Virgo.

Using observations of specially assembled samples, the morphology of *isolated* E/S0 has been studied recently by Colbert et al. (2001), who find that shells and tidal features are

Table 3. Morphology and basic E scaling relations calculated with SBF distances. *Law* law tested, i.e. FP Fundamental Plane, FJ Faber-Jackson; *Sbs* subsample, i.e. *Nop* "normal" E with $\Sigma_2 \leq 1$, *Pec* "peculiar" E with $\Sigma_2 > 1$, *un*E, *di*E, *bo*E; *N* number of objects; *mRes* mean residual; σ standard deviation.

Law	*Sbs*	*N*	*mRes*	σ
FP	*Nop*	61	0.00 ± .02	0.15
FP	*Pec*	28	−0.16 ± .04	0.23
FP	*un*E	34	0.00 ± .03	0.17
FP	*di*E	36	−0.08 ± .03	0.19
FP	*bo*E	19	−0.06 ± .04	0.18
FJ	*Nop*	61	0.00 ± .07	0.54
FJ	*Pec*	28	−0.36 ± .12	0.62
FJ	*un*E	34	−0.13 ± .10	0.61
FJ	*di*E	36	−0.10 ± .10	0.59
FJ	*bo*E	19	−0.13 ± .13	0.59

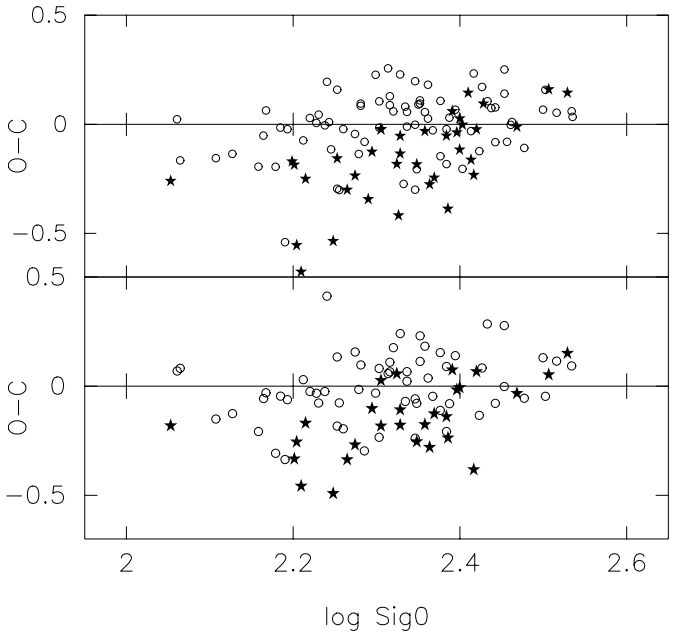

Fig. 4. Residuals of sample galaxies from the Fundamental Plane. Circles: "normal" galaxies or *Nop* sample. Stars: "peculiar" or *Pec* sample. The constant in the FP equation is adjusted to give a mean residual of 0.0 for the *Nop* subsample. *Upper frame*: PS96 distances. *Lower frame*: SBF distances.

"much more prevalent" in such an environment than in compact groups.

It should be noted that the proportion of "peculiar" is approximately the same in the three subsamples of *un*E, *di*E and *bo*E, respectively 33, 29 and 37%, against 33% for the full sample. The difference between the proportion for disky and boxy Es is of doubtful significance. This may be an argument against the systematic use of boxyness as one of the criteria of peculiarity. There are however cases of extreme boxyness, such as NGC 3640 (Fig. 1) or IC 3370 (Fig. 3)

We have finally verified that the proportion of morphologically peculiar Es does not significantly depend upon their luminosity (or σ_0), at least within the limitations of the present data.

3.4. Correlations between morphology and the basic E properties

We have considered the basic structural properties of E-galaxies separately for the normal and peculiar objects as defined here, and also separately for the 3 recognized sub-types. We derive a basic relation for the *Nop* subsample, i.e. our objects with $\Sigma_2 \leq 1$, and calculate the deviations from this relation for the other subsamples of interest.

1. *Fundamental Plane (FP):* We adopt the definition of the FP in PS96, Eq. (4), that is:

   $$\mathrm{O{-}C} = 2\,\log\sigma_0 + 0.286\,M_B + 0.2\,\mu_e - C_0.$$

   We introduce small modifications of the constant term C_0, in order to nullify the mean residual for the *Nop* subsample alone. Using the SBF distances we then find the results of Table 3, while the residuals of the *Nop* and *Pec* subsample from the FP are compared in Fig. 4. *It appears that the above defined "peculiar" Es, the Pec subsample, is systematically offset from the FP defined by the "normal" Es.They thus introduce a significant extra dispersion in the quality of the FP fit, when obtained in the usual way, i.e. without distinguishing between "normal" and "peculiar" Es.* On the other hand no convincing differences appear between the 3 sub-types of *un*E, *di*E, *bo*E.
2. *Faber-Jackson relations (FJ):* The 61 objects in the *Nop* sample define the FJ relation, using the SBF distances, with a scatter $\sigma = 0.54$. The statistics of residuals for other subsamples are in Table 3. The FJ distributions for the *Nop* and *Pec* samples are shown in Fig. 5. Clearly "peculiar " Es are too bright, at a given velocity dispersion, by 0.36 in the mean. This excess luminosity, as well as the deviations of *Pec* galaxies from the "normal" FP, should probably be explained by changes of the surface-brightness, already discussed in SS92.

   On the other hand, the 3 sub-types are quite equivalent as regards the FJ relation: since each of these subsamples contains grossly 1/3 of peculiar objects, they deviate from the "normal" galaxies by roughly 1/3 of the mean deviation for the *Pec* subsample.

   The results collected in Table 3 are found from the set of 89 objects with known SBF distances. Using the full set of 114 galaxies with the PS96 distances, quite similar results are obtained, with slightly larger dispersions, as shown in Figs. 4 and 5. An attempt has been made to improve the set of absolute magnitudes by averaging the data from the here used sources (after allowance for the above quoted systematic difference), but no significant changes of the results occur.
3. *Dust contents:* Since their dust content may be a possible clue of the past evolution of galaxies, the IRAS fluxes distributions for the *Pec* and the *Nop* samples have been intercompared, using the data from Knapp et al. (1989).

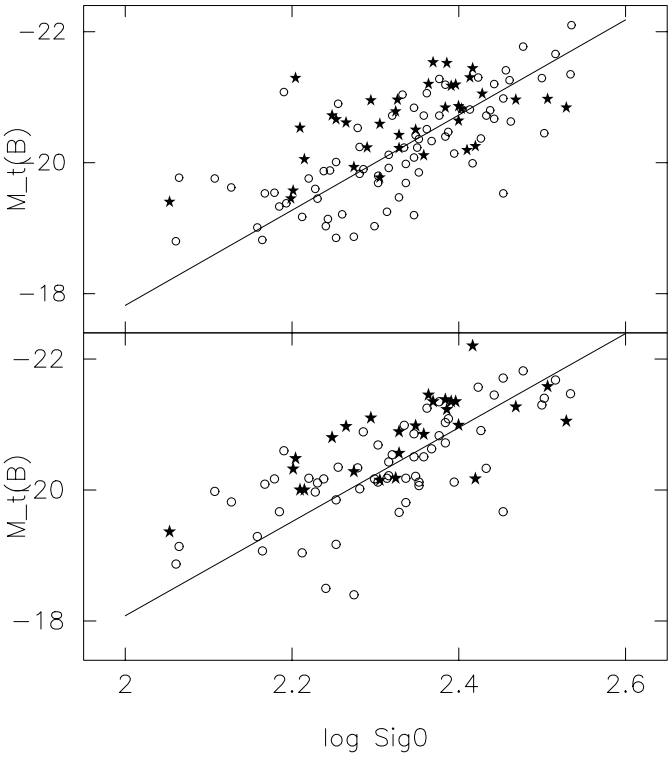

Fig. 5. The Faber-Jackson relation for the sample galaxies. Circles: *Nop* subsample. Stars: *Pec* subsample. The lines are impartial fits to the *Nop* sample. *Upper frame*: PS96 distances. *Lower frame*: SBF distances.

The raw fluxes were corrected for differences in distances, using the PS96 distance moduli, so that all objects were brought to the distance of Virgo. The distributions of the 100 μ fluxes are given in Table 4 for the two subsamples. The 100 μ brightest E objects are slightly more frequent in the *Pec* subsample than in the *Nop* one: 25% against 17% for the two upper steps of the distribution together. In view of the small numbers of dusty objects, this is an indication of marginal significance.

4. *Kinematically Distinct Cores (KDC):* The Kinematically Distinct Cores in ellipticals have often been explained as traces of past interactions and mergers (see reviews by de Zeeuw & Franx 1991). If these events were the same as those leading to morphological peculiarities, a one to one relation between the two kind of "signatures", i.e. morphological and kinematical, would have long been found. The situation seems to be the opposite: for instance, Bettoni (1992) points out that NGC 2865, with its many shells and fan extensions ($\Sigma_2 = 10.6$), has quite normal kinematics. Similarly NGC 5982 ($\Sigma_2 = 6.8$) is qualified of "smooth triaxial galaxy" after a careful discussion of its kinematics (Oosterloo et al. 1994). On the other hand, objects with well known KDC's, such as NGC 3608, 4365, IC 1459 and others are devoid of morphological peculiarities. See also the search of photometric peculiarities in KDC objects by Carollo et al. (1997), with negative results.
This question has been tackled anew by a systematic comparison of KDC occurences in the *Pec* and *Nop* samples.

Table 4. Distribution of the IRAS 100 μ fluxes for *Nop* and *Pec* ellipticals. The fluxes $S_V(100)$ are reduced to the distance of the Virgo cluster. (1) Subsample; (2) N number of objects with data; (3) % in $S_V(100)$ range 0−250; (4) % in 250−500; (5) % in 500−1000; (6) % in 1000−2000; (7) % in 2000−4000; (8) % in range >4000.

(1)	(2)	(3)	(4)	(5)	(6)	(7)	(8)
Nop	73	49 ± 8	10 ± 4	14 ± 4	10 ± 3	12 ± 3	5 ± 2
Pec	36	46 ± 10	16 ± 6	5 ± 3	8 ± 3	14 ± 6	11 ± 5

Table 5. Kinematically Distinct Cores (*KDC*) in *Nop* and *Pec* ellipticals. Velocity profiles are classified in 5 groups: *Und* (eterminate); sure *KDC*; uncertain *KDC*:; *Nof* (eature); *Nof*:; *Und* (eterminate). The table gives the number of objects in each group and totals, separately for the *Nop* and *Pec* subsamples.

Sample	*N*	*KDC*	*KDC*:	*Nof*	*Nof*:	*Und*
Nop	69	10	4	34	7	14
Pec	32	4	2	17	3	6

Since such occurences are not very straightforward, we examined the available graphs of rotation velocities for each object, using the list of references in the HYPERLEDA data base, and classified these as follows:
Und if the velocities are too small (or the data too poor) to decide if a KDC is present or not (Ex: NGC 5846).
KDC if such a feature is certainly there (Ex: IC 1459)
KDC: if the presence of such a feature is likely but remains uncertain (Ex: NGC 4478)
Nof if no KDC feature seems possibly present (Ex: NGC 3379 and most *di*E)
Nof: if the absence of a KDC feature is likely but remain uncertain (Ex: NGC 1549). The difference between the *KDC*: and *Nof*: subdivisions is a matter of feeling!
The distribution of our samples into these 5 categories is presented in Table 5. It appears that the distributions for the *Pec* and *Nop* subsamples are not significantly different. KDC's, certain or probable, are no more frequent in morphologically peculiar ellipticals than in their undisturbed sisters. Although 2D kinematics at high resolution may often be necessary to unveil peculiar velocity fields (see Hau et al. 1999; Wernli et al. 2001) it is not clear how the limitations of the here used data might affect this conclusion. *The events leading to either morphological or kinematical peculiarities cannot be directly related.*

4. Morphology and stellar populations

The stellar populations of "peculiar" (*Pec* subsample) have been compared to those of "normal" Es (*Nop* subsample), using the colour indices $U-B$, $B-V$, $B-R$, $V-I$, and the line indices Mg_2, Hβ, $\langle$Fe$\rangle$ and Mgb. For this purpose, *the correlations, for the Nop subsample, between population indices and the galaxy mass, measured by the central velocity dispersion σ_0 have been taken as references.* These correlations are very tight for the colours and the Mg_2 or Mgb indices, but poorer for

Table 6. Population of the "normal" Es (*Nop* subsample). The correlations between the central velocity dispersion and various population indices are given in the form $y = px + y0$, where $x = \log \sigma_0$ (1) Index; (2) number of objects (not taking into account the 1 to 3 rejected by the least squares routine); (3) slope p; (4) intercept y_0; (5) standard deviation σ; (6) coefficient of correlation ρ. The line indices Hβ, ⟨Fe⟩, Mgb are here in magnitudes.

Index	N	p	y_0	σ	ρ
$B-V$	77	$0.194 \pm .026$	$+0.485 \pm .003$	.025	0.65
$U-B$	76	$0.452 \pm .040$	$-0.543 \pm .004$	.036	0.80
$U-V$	76	$0.765 \pm .057$	$-0.333 \pm .006$	.054	0.77
$B-R$	75	$0.258 \pm .049$	$+0.910 \pm .005$	.046	0.53
$V-I$	68	$0.180 \pm .048$	$+0.777 \pm .005$	.042	0.42
Mg_2	77	$0.182 \pm .017$	$-0.133 \pm .002$	.016	0.78
Hβ	57	$-0.022 \pm .006$	$+0.116 \pm .001$	.007	0.36
⟨Fe⟩	63	$0.022 \pm .004$	$+0.031 \pm .001$	.005	0.46
Mgb	61	$0.095 \pm .010$	$-0.048 \pm .001$	.012	0.69

the Hβ and ⟨Fe⟩ indices. The equations for the direct correlations $y = px + y0$, where $x = \log \sigma_0$ and y is one of the population indices are given in Table 6, and also plotted on the correlation diagrams of Figs. 6 and 7. The colours and line-indices do not refer to the same volume in a given galaxy: colours are integrated in the circle of radius r_e, while line-indices are measured in near center small areas. This should have no influence on our conclusions, because only *residual indices* between *Pec* galaxies values and the *Nop* sample are considered.

The present results for the *Nop* sample may be compared with previous work on cluster galaxies (Jorgensen 1999; Kuntschner 2000) or mixed samples (Kuntschner et al. 2001). Kuntshner (2000) uses precise observations of a small sample in Fornax and compares his results with previous data. Our regressions for the *Nop* sample in Table 6 are generally in excellent agreement with this author (his Table 5). For ⟨Fe⟩ we obtain the adequate representation by averaging Kuntschner's regressions for the two relevant Fe-lines: our slope is then slightly smaller.

The residuals, from these references relations, of population indices in various subsamples of interest have then been studied. These quantities will be called below "residual indices" for brevity. Among such subsamples, we primarily consider the *Pec* one: the residuals for *Pec* galaxies are listed in Table 7, and their statistics for this subsample are given in Table 8. Figure 8 illustrates the relations between residuals, for part of the indices, and the Σ_2 peculiarity index. Incidentally, population indices for the three sub-types *un*E, *di*E, *bo*E have also been considered, but the results will not be discussed here.

For morphologically peculiar E galaxies, the results are the following:

1. *"Peculiar" objects* (*Pec* sample) often have slightly bluer *UBVRI* colours than the reference sample of "normal" (or *Nop*). The average Mg_2 index is also slightly smaller for the *Pec* subsample than for the *Nop* one, and this is also clearly the case for the Mgb index. The reverse is true for the average Hβ index which is larger for the *Pec* than for the *Nop* galaxies. These are indications for the presence of a younger population in *Pec* objects. It appears however, from Figs. 6 and 7, that the σ_0-Indices relations for the *Pec* and *Nop* subsamples *are largely mixed. This mixing is nearly complete for giant galaxies of large σ_0: population anomalies mainly occur for lesser objects*. There is another surprising feature in Fig. 6 or Table 8: the $U-B$ indices of *Pec* objects remain much closer from the *Nop* regression than is the case in $B-V$, while the reverse would be expected for a straightforward age effect.
2. *Correlations with Σ_2?* In Fig. 8 are plotted the eventual correlations between the peculiarity index Σ_2 and the residuals of the $U-B$, $B-V$ and line-indices of the *Pec* galaxies from the regression adequate for the *Nop* subsample. Such correlations were found in SS92 and Schweizer et al. (1990), but are not confirmed from our larger sample. The reason of this discrepancy lies in the behaviour of several well known

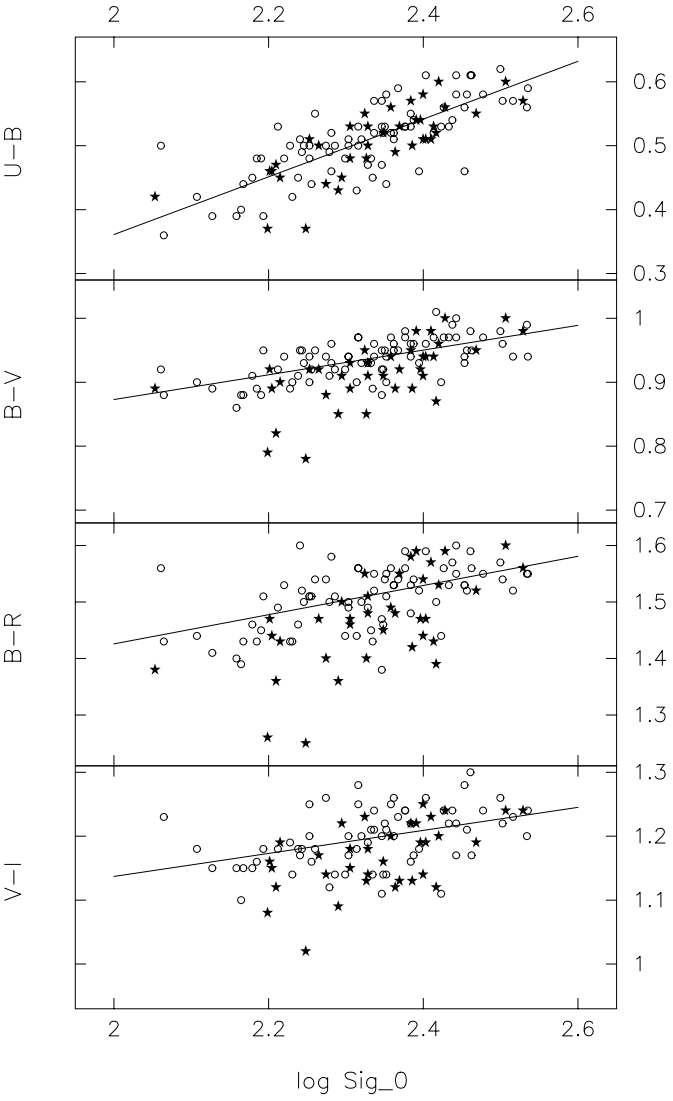

Fig. 6. The Colour–σ_0 relations for *Nop* galaxies (circles and fitted lines), and *Pec* objects (stars). Part of the "peculiar" objects tend to be bluer than "normal", much less so in $U-B$ (*upper panel*) than in $B-V$, $B-R$ and $V-I$. Both categories of objects appear well mixed in the high mass range.

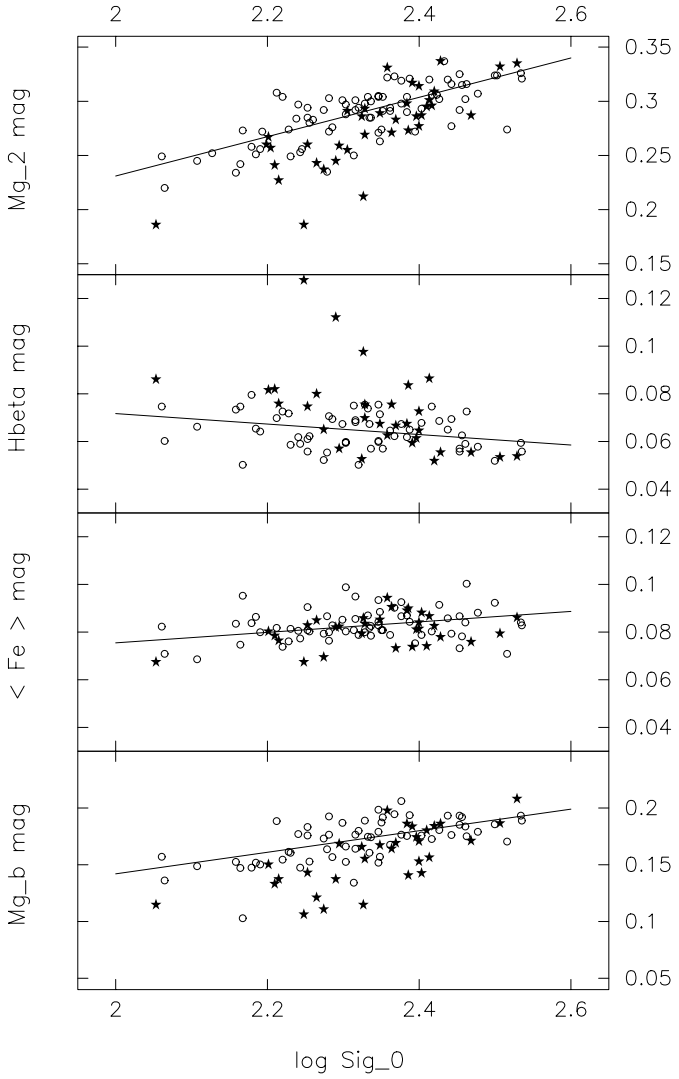

Fig. 7. The Line Indices–σ_0 relations for *Nop* galaxies (circles and fitted lines), and *Pec* objects (stars). All indices are here given in magnitudes, as usual for Mg_2. The Indices–σ_0 relations for the *Nop* subsample are all fairly good, as usually found for cluster galaxies. The "peculiar" objects introduce most of the scatter. They deviate systematically, except perhaps the most massive, with fainter spectral features in Mg_2 and Mg_b, a stronger Hβ line, while the $\langle$Fe$\rangle$ index is nearly unchanged (although often fainter).

"peculiar" Es, such as NGC 1344, 1549, 3923 and 4552, which have nearly the same populations indices as "normal" objects of the same σ_0. In place of a correlation there remains a loose trend, with a number of "peculiar" Es also anomalous as regards their stellar populations. One may quote NGC 1700, 2865, 3557, IC 3370, NGC 4976, 5018, 5061, 5576, 5982 as objects with large Σ_2, notable blueing and line-indices revealing a younger stellar population.

Clearly, the Pec galaxies may be sorted out in two families, noted respectively YP and NP in Table 7. In the first one, are objects with consistent evidence for the admixture of a younger population in the stellar mix. The second one contains objects with an apparently normal (or reddish) population from the available indices. Galaxies with little morphological peculiarities, i.e. small Σ_2, are often in the *NP* class. This classification has been obtained simply by looking at the residuals in Table 7, neglecting however those in $\langle$Fe$\rangle$ which seem to be much less sensitive to peculiarities than the others.

Considering only the 25 galaxies in the *Pec* subsample with $\Sigma_2 \geq 3$, there are 9 in the first family, with a near normal population: this includes NGC 3923, the queen of shell galaxies! Several of these are reddish, perhaps as evidence of enhanced metallicity. There are 11 in the second class, with consistent evidence for "rejuvenation", including NGC 2865, a very peculiar object indeed. Finally 5 are doubtful cases, with conflicting evidence from various indices. NGC 5322 is an interesting galaxy, with little morphological peculiarity, but consistent evidence for a population anomaly.

For $\Sigma_2 \geq 5$ however, the proportion of *YP* objects increases dramatically: among the 12 objects so indexed, we find only 3 of the *NP* population brand, 2 of these being considered uncertain.

3. *Recent interactions and the nature of intruders*: Assuming now that morphological peculiarities result from a relatively recent interaction of a pre-existing E-galaxy with a much smaller object, can we get some indication upon the nature of this intruder?
   - *Nearly half of the Pec sample are in the above defined NGC 3923 or NP family with normal, or reddish, populations.* Two qualitative explanations may be offered: either no young star formation occured in connexion with the development of the shells and/or asymmetries (and captured stars, if any, were of the old brand characteristic of E-S0); or stars were formed in a not too recent past *and from a metal-rich ISM*, in such a way that their larger metallicity could compensate their relative youth. Among objects in this class we find NGC 4552 in Virgo or NGC 1344 in Fornax (a doubtful case however), with an ample supply of possible intruders, either of early-type or metal rich.
   - *For the other family, whose NGC 2865 is the most extreme example, the population anomalies are evident from the indices here studied and qualitatively consistent with the formation, or capture, of some amount of young stars.* Objects of the *YP* family seem to be particularly scarce in a cluster environment, with none in Virgo and one doubtful case in Fornax.
4. *A mean index of younger population*. In their discussion of the tilt of the FP, Prugniel & Simien (1997) introduced "a combined stellar population indicator", based on colours and Mg_2. A somewhat similar approach is adopted here, because a glance at the residuals in Table 7 show these to be intercorrelated for a given object, specially for *YP* galaxies. This evidence led us to define *an ad hoc "mean index of younger population" (MIYP)*, for objects in the NGC 2865 family and others. *This index is a weighted mean of the measured residuals of Table 7, all expressed in magnitudes*, with weights 1 for $B-V$ and $U-B$, 5/3 for Mg_2 and Mgb, and -3 for Hβ. The $\langle$Fe$\rangle$ residual was neglected because of its very modest response to peculiarities, and the $B-R$ and $V-I$ ones because they would give an unwanted weight

Table 7. Residuals of colours- and line-indices of ellipticals in the *Pec* subsample, against the standard relations calculated for the *Nop* subsample between Indices and the central velocity dispersion. (1) Name; (2) Σ_2 index of peculiarity; (3) $\Delta B-V$, $B-V$ residuals; (4) $\Delta U-B$, $U-B$ residuals; (5) $\Delta B-R$, $B-R$ residuals; (6) $\Delta V-I$, $V-I$ residuals; (7) ΔMg_2, Mg_2 residuals; (8) $\Delta H\beta$, $H\beta$ residuals in (Å; (9) $\Delta\langle Fe\rangle$, $\langle Fe\rangle$ residuals in Å; (10) ΔMgb, Mgb residuals in Å; (11) "Mean Index of Younger Population" or *MIYP* (see definition in text) in mag; (12) character of population: YP, Young Population present, NP, probably normal population, : doubtful.

Name	Σ_2	$\Delta B-V$	$\Delta U-B$	$\Delta B-R$	$\Delta V-I$	ΔMg_2	$\Delta H\beta$	$\Delta\langle Fe\rangle$	ΔMgb	*MIYP*	Pop
NGC 0596	2.1	−0.015	−0.009	−0.051	0.014	−0.043	0.24	0.04	−0.76	−0.033	YP
NGC 1344	5.4	−0.023	0.006	−0.038	−0.024	−0.011	–	–	–	−0.012	NP:
NGC 1395	3.8	−0.011	0.037	0.012	0.041	0.010	0.05	−0.22	−0.27	0.004	NP
NGC 1399	2.0	0.004	−0.031	−0.001	0.008	0.008	−0.16	−0.33	0.48	0.006	NP
NGC 1537	2.2	0.008	0.007	−0.007	−0.013	−0.001	0.37	0.15	−0.33	−0.009	NP
NGC 1549	7.0	−0.007	−0.010	−0.030	−0.016	0.002	0.29	–	–	−0.012	NP:
NGC 1653	3.5	−0.011	−0.034	−0.059	−0.020	−0.017	–	0.01	−1.13	−0.034	YP
NGC 1700	3.8	−0.058	−0.036	−0.105	−0.077	−0.028	0.52	0.11	−1.16	−0.053	YP
NGC 2768	1.2	−0.020	−0.045	−0.001	0.030	−0.026	−0.21	0.04	−0.03	−0.017	NP:
NGC 2865	10.6	−0.141	−0.104	−0.239	−0.162	−0.090	1.57	−0.41	−1.81	−0.135	YP
NGC 2974	3.6	0.014	0.041	0.041	0.034	−0.004	−0.32	−0.15	−0.21	0.015	NP
NGC 3557	4.3	−0.084	−0.030	−0.143	−0.092	−0.011	–	–	–	−0.044	YP
NGC 3585	2.8	−0.031	0.001	−0.065	−0.040	−0.005	0.08	0.01	−0.24	−0.012	YP:
NGC 3610	6.8	−0.094	0.013	−0.119	−0.055	−0.028	0.39	0.07	−0.88	−0.059	YP
NGC 3613	1.7	−0.027	0.020	0.001	−0.056	−0.022	0.13	0.01	−0.54	−0.018	YP:
NGC 3640	8.8	−0.004	0.018	−0.036	−0.023	−0.015	0.37	0.18	−1.41	−0.046	YP
NGC 3923	10.3	0.003	0.035	0.056	0.024	−0.003	0.11	0.07	0.24	0.018	NP
NGC 4125	2.5	−0.025	0.001	0.030	−0.074	−0.015	0.08	−0.48	−0.24	−0.014	YP
NGC 4374	2.1	−0.014	−0.026	−0.032	−0.024	−0.029	−0.16	−0.59	−0.45	−0.019	YP:
NGC 4406	3.1	−0.030	−0.001	−0.057	−0.019	−0.017	−0.05	−0.22	−0.15	−0.012	NP:
IC 3370	7.7	−0.042	−0.020	−0.044	−0.012	−0.032	–	–	–	−0.038	YP
NGC 4552	3.9	0.006	0.048	−0.003	−0.013	0.002	−0.29	−0.22	0.09	0.019	NP
NGC 4767	3.3	−0.002	0.030	−0.034	−0.042	0.004	–	–	–	0.012	NP:
NGC 4976	5.2	−0.122	−0.082	−0.216	−0.093	−0.007	–	–	–	−0.072	YP
NGC 5018	8.0	−0.086	−0.029	−0.109	−0.066	−0.078	0.86	0.07	−1.78	−0.088	YP
NGC 5061	3.2	−0.079	−0.063	−0.140	−0.099	−0.039	1.22	0.04	−0.97	−0.080	YP
NGC 5077	4.8	0.027	−0.037	0.039	0.019	−0.011	–	−0.52	−0.03	−0.008	NP
NGC 5322	2.6	−0.054	−0.036	−0.039	−0.083	−0.026	0.32	0.18	−0.36	−0.038	YP
NGC 5557	6.7	−0.013	−0.019	−0.102	−0.047	−0.005	0.63	−0.07	−0.76	−0.031	YP
NGC 5576	8.0	−0.046	−0.046	−0.096	−0.047	−0.044	−0.03	−0.41	−1.75	−0.065	YP
NGC 5846	4.2	0.031	0.001	0.064	0.012	0.015	−0.11	−0.48	0.15	0.015	NP
NGC 5982	6.8	−0.041	−0.033	−0.088	−0.069	−0.027	0.26	−0.15	−0.82	−0.039	YP
NGC 6411	3.0	−0.002	0.034	–	–	−0.017	0.21	0.15	−0.70	−0.023	YP:
NGC 7454	2.5	0.007	0.034	−0.059	–	−0.055	0.39	0.02	−0.97	−0.030	YP:
NGC 7507	4.6	−0.002	0.036	−0.027	−0.002	0.035	−0.03	0.33	0.65	0.026	NP
NGC 7619	2.8	0.029	0.009	0.044	0.012	0.009	−0.19	−0.56	−0.09	0.014	NP
NGC 7626	1.4	0.044	0.005	0.055	0.026	0.028	−0.19	−0.44	0.12	0.025	NP

to strongly correlated colours. Note that *MIYP* < 0 for objects bluer (younger) than the "normal" Es. The *MIYP* may be used as a substitute of the various residual indices with improved accuracy: it is based upon 5 measured indices, and it seemed feasible to cancel from the mean a few anomalous data, i.e. the $\Delta U-B$ residuals for NGC 3610 and 3640 and the $\Delta H\beta$ for 5576. This composite index is not statistically different from the $\Delta B-V$. For the *Nop* subsample this index has a mean value of −0.0006, in agreement with its definition, and a standard deviation of 0.019 (no rejections). This may be compared with the dispersions of individual indices about the relevant regressions (Table 6), weighting these as in the definition of *MIYP*. Errors in $U-B$ are the main source of errors in *MIYP*.

Table 8. Mean deviations of the population indices of morphologically peculiar Es (*Pec* subsample) against the standard relations calculated for the *Nop* ("normal") subsample. *Ind* index studied; *N* number of objects; *mRes* mean residuals; σ standard deviation. Mean residuals for the indices Hβ, ⟨Fe⟩, Mg*b* are in Å.

Ind	*N*	*mRes*	σ
$B-V$	37	$-0.025 \pm .008$	0.049
$U-B$	37	$-0.008 \pm .006$	0.037
$U-V$	37	$-0.034 \pm .014$	0.078
$B-R$	36	$-0.044 \pm .014$	0.085
$V-I$	34	$-0.030 \pm .009$	0.055
Mg_2	37	$-0.017 \pm .005$	0.030
Hβ	30	$+0.22 \pm .10$	0.49
⟨Fe⟩	31	$-0.07 \pm .05$	0.23
Mg*b*	31	$-0.47 \pm .15$	0.76

Figure 9 shows the relations between the Σ_2 peculiarity index and the defined population index *MIYP*, to be compared with the graphs of Fig. 8 for the various population indices: the dichotomy between the *YP* and *NP* families is more clearly seen and a better correlation appears between the two ad hoc indices for the *YP* family. Note that objects of the *NP* family tend to be reddish, i.e. $MIYP > 0$.

In Fig. 10 we trace the relation between the FP residuals for the *Pec* subsample, as calculated in Sect. 3.4 and displayed in Fig. 4, and the *MIYP*. There is a rough correlation, sufficient to confirm that the residuals from the FP for these objects are indeed due to their population anomalies, leading to a lesser M/L for *YP* galaxies (O−C < 0 in magnitudes). The *NP* objects, with a normal or reddish population, tend to lie in the FP (often O−C > 0 in magnitudes). with the exception of NGC 1344.

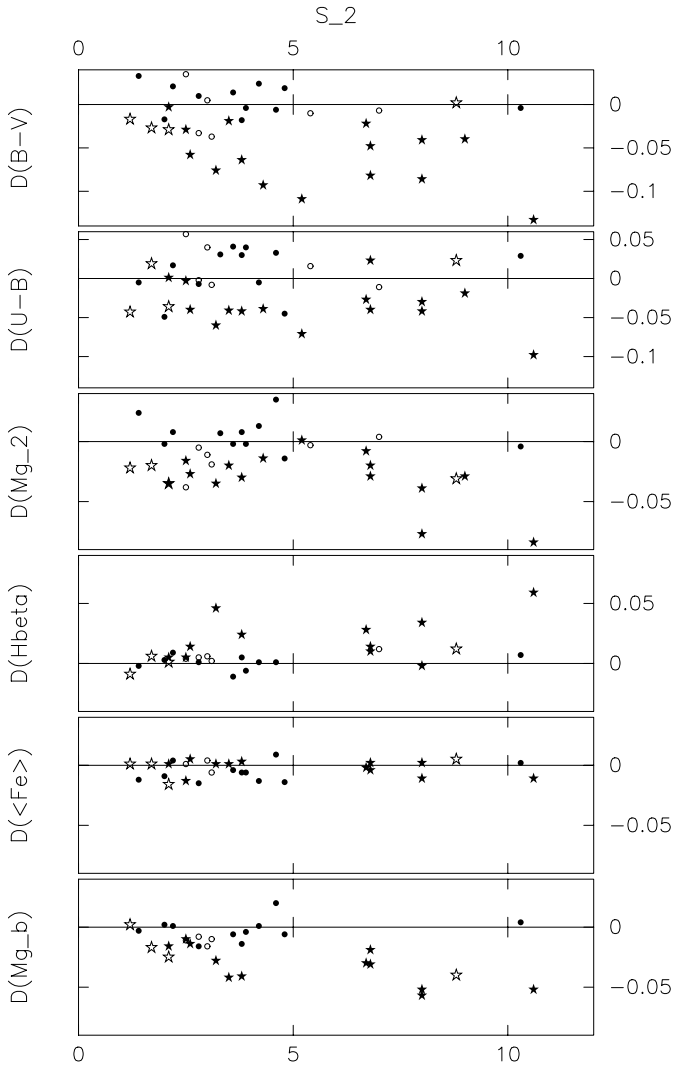

Fig. 8. Abscissae: the Σ_2 index of peculiarity. Ordinates: colour and line-indices residuals of galaxies in the *Pec* subsample against the Indices–σ_0 relations defined by the *Nop* subsample. From top to bottom, residuals for $B-V$, $U-B$, Mg_2, Hβ, ⟨Fe⟩, Mg*b*. The last 3 indices are expressed in magnitudes. The objects have been sorted out into the two families *YP* (young population present) and *NP* (normal or reddish population) as tabulated in Table 7. Symbols: Star *YP*. Heavy dot: *NP*. Open star: uncertain *YP*. Light circle: uncertain *NP*.

5. Concluding discussion

5.1. Summary of results

– Using an objective definition of morphological peculiarities, it is found that "peculiar" ellipticals (*Pec* subsample) number about 1/3 of the total sample of 114 objects, mostly in poor and loose groups. This proportion decreases in denser environments, such as the Virgo cluster, specially if the importance of the morphological perturbations is considered (Table 2). In Virgo, only NGC 4552 (Malin 1979) displays shells and one outer jet, out of the 16 Es here studied. On the other hand, no changes of the occurence of peculiarities were found in connection with the E subtypes (*di*E, *bo*E, *un*E) or luminosities.

– The *Pec* galaxies systematically deviate from the Fundamental Plane optimized for the "normal" *Nop* objects (Table 3, Fig. 4). They are also "too bright" according to the Faber-Jackson relation (Table 3, Fig. 5). Such deviations from the basic scaling relations are due to an admixture of younger stars in part of the *Pec* objects: this is shown by the correlation of Fig. 10 between the ad hoc *MIYP* index and the residuals of *Pec* galaxies above the Fundamental Plane. Closely related results are obtained by Prugniel et al. (1999) who plot residuals to the FP and to the $Mg_2 - \sigma_0$ relation, against their calculated local density (see also Kuntschner et al. 2002).

– The dust contents, as measured from the IRAS 100 μ fluxes have quite similar distributions in the *Pec* and *Nop* subsamples of galaxies.

– The frequency of occurence of Kinematically Distinct Cores seems to be the same in the *Pec* and *Nop* subsamples, showing that the events leading to kinematical and morphological peculiarities are probably unrelated. This applies to the major KDC considered in the present statistics. The picture might change when very minor kinematic features will be considered.

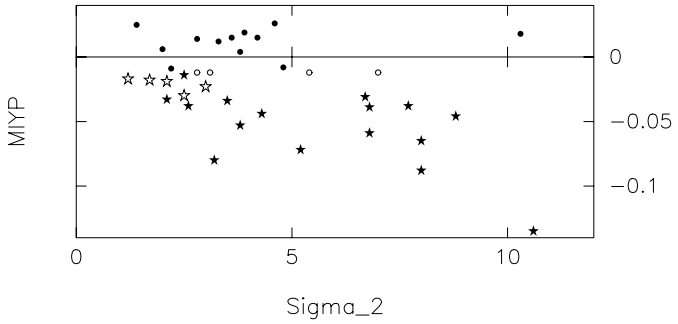

Fig. 9. Abscissae: the Σ_2 index of peculiarity. Ordinates: the Mean Index of Younger Population, or *MIYP* defined in Sect. 4.4. Symbols: *YP* objects, full stars; *NP* objects, full dots; uncertain *YP*, open stars; uncertain *NP*, open circles. The dichotomy between the two *YP* and *NP* families of peculiar Es (see Sect. 4.2) is more marked than in Fig. 8.

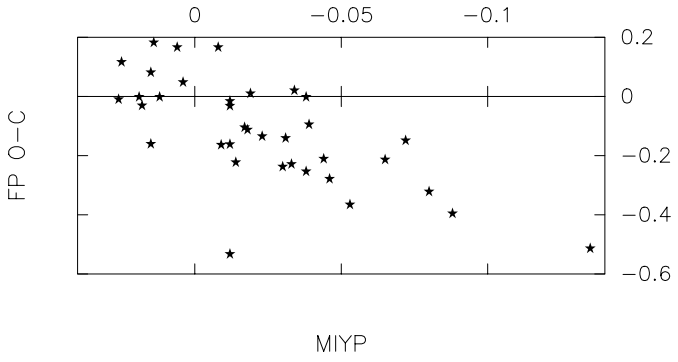

Fig. 10. Abscissae: the *MIYP* mean index evidencing the inclusion of a younger population (Sect. 4.4). Ordinates: residuals from the Fundamental Plane (see also Sect. 3.4, Fig. 4), with the PS96 distances. The correlation is spoilt by an outlier, i.e. NGC 1344, which is classified in the NP: family, as showing no evidence of a young population, but deviates badly from the FP of "normal" galaxies.

– From available colour- and line-indices, many *Pec* galaxies show evidence of "pollution" by relatively young stars, which confirm the classical result in SS92 and related papers. These population "anomalies" have been studied from "residual indices", i.e. differences of actual indices from the reference values predicted by the Index-log σ_0 relations established for the *Nop* sample. At variance with the classical results however, no clear correlations are found between these residuals and the peculiarity index Σ_2. Indeed a significant proportion of *Pec* objects (more than 1/3 and not much less than 1/2), have *normal (or reddish) stellar populations*, including such famous cases of peculiarity as NGC 3923 or 4552. This phenomenon was apparently overlooked before, perhaps due to unsufficient samples.
  The *Pec* objects have thus been tentatively sorted out in two families: in the first, or *YP*, galaxies have experienced the formation, or capture, of some proportion of much younger stars than the standard E old population. The second, or *NP* one, with normal or reddish population, might result from interactions between old galaxies, devoid of sufficient ISM for new star formation, or alternatively from the admixture of stars of medium age and high metallicity. *YP* objects are more frequent among galaxies with larger Σ_2 (those with more extreme peculiarities).

5.2. Discussion

It should be emphasized that, from the morphological point of view alone, the ellipticals of the *Pec* subsample form a very heterogeneous group: part of them show only modest deviations from the accepted E symmetry, while other display rather chaotic outer structures. These differences are perhaps poorly summarized in the Σ_2 index. Similarly the populations of these "peculiar" are not homogeneous, and several schemes of interactions are possible, or necessary, to explain the resulting properties.

– The event leading to the present morphological peculiatities and population deviances might be a major merger, bringing the pair, after violent relaxation, to the present "nearly E-type" characteristics, but with persisting outer "non-elliptical" structure. We suspect that NGC 3640 or IC 3370 might be among such objects: they present relatively small population indices residuals. It would be feasible to derive, from the here collected colour- and line-indices, so-called "heuristic" ages of the event (see SS92), or "SSP ages" of the resulting population as in Trager et al. (2000), or perhaps use a more elaborate method to characterize a composite population resulting from a 5−7 Gyr old major burst.
– The event might rather be a minor merger, involving an already fully developed elliptical with its characteristic old population, plus another object leaving part of its stars, or eventually being fully captured, or providing its ISM for a burst of stellar formation. Then one may consider as significant the *residuals of populations indices* from the usual indices of early-type galaxies as described by the *Nop* sample: the residuals directly result from stars acquired during the interaction, and may provide some clues of the nature and origin of this added population. For the *YP* (or NGC 2865) family, one would like to know more about the young stars formed or capured during the event: age, metallicity, perhaps origin. We may guess from population indices that this event was quite recent, younger than 1 Gyr, and the morphology of such objects as NGC 2865 or 5018 support this idea.
– Some members of the *NP* (or NGC 3923) family, have complex sysstems of shells of low mass and probably great persistence. These might again result from a minor merger, the star formation event occuring in a more distant past, or eventually involving a material of enhanced metallicity. This might explain the nearly unchanged or reddened populations as compared to the standard E.
– Finally some objects, like NGC 5846, or 1395 or 4406 show essentially pure tidal distorsions, probably resulting from gravitational interaction with a minor early-type object. Their population is necessarily in the *NP* family.

Exploratory calculations have been made to get some insight in the problem by summing old E-type populations with minor proportions of stars in the 0.5−3 Gyr age range and

Table 9. Exploratory models of the populations of two prototypical *Pec* galaxies, i.e. NGC 2865 and NGC 3923. Observed residual indices are taken from Table 7, with probable errors from the fits for *Nop* galaxies (Table 6). The models are sums of an old *Nop* object with population indices obtained from the observed $\log \sigma_0$ and the regressions in Table 6, plus a recent SSP by Bressan et al. (1994, 1996) (B*al*) or by Worthey (1994) (W94) and fractional V luminosity k_V. (1) Source; (2) $\Delta B - V$; (3) $\Delta U - B$; (4) $\Delta B - R$; (5) $\Delta V - I$; (6) ΔMg_2; (7) $\Delta H\beta$; (8) $\Delta\langle Fe\rangle$; (9) $\Delta Mg b$.
Sources for models: N2865 Mod. A: SSP by B*al*, A = 1 Gyr, Z = 0.008, k_V = 0.4.
N2865 Mod. B: SSP by B*al*, A = 0.75 Gyr, Z = 0.008 (line indices extrapolated), k_V = 0.3.
N2865 Mod. C: SSP by B*al*, A = 0.5 Gyr, Z = 0.008 (no line indices available), k_V = 0.23.
N3923 Mod. A: SSP by B*al*, A = 3 Gyr, [Fe/H] near 0.4, k_V = 0.3.
N3923 Mod. B: SSP by W94, A = 3 Gyr, [Fe/H] near 0.4, k_V = 0.3.

Source	$\Delta B - V$	$\Delta U - B$	$\Delta B - R$	$\Delta V - I$	ΔMg_2	$\Delta H\beta$	$\Delta\langle Fe\rangle$	$\Delta Mg b$
N2865 Obs.	−.141 ± .025	−.104 ± .036	−.239 ± .046	−.162 ± .042	−.090 ± .016	+1.57 ± .19	−0.41 ± .19	−1.81 ± .35
N2865 Mod. A	−0.132	−0.135	−0.159	−0.053	−0.060	+0.93	−0.55	−0.99
N2865 Mod. B	−0.139	−0.123	−0.174	−0.058	−0.052	+1.00	−0.48	−0.83
N2865 Mod. C	−0.142	−0.136	−0.209	−0.057	–	–	–	–
N3923 Obs.	+.003 ± .025	+.035 ± .036	+.056 ± .046	+.024 ± .042	−.003 ± .016	+0.11 ± .19	+0.07 ± .19	+0.24 ± .35
N3923 Mod. A	+0.007	+0.008	+0.054	+0.093	−0.007	+0.12	−0.14	−0.45
N3923 Mod. B	+0.026	+0.030	+0.036	+0.028	−0.006	+0.03	+0.02	−0.26

various metallicities. To describe the old populations it seemed reasonable, by analogy to the above empirical comparisons, to use the observed colours and line-indices summarized by the regressions of Table 6. The injected stars were described by SSP models. Both the SSP's by Worthey (1994) and those by Bressan et al. (1994, 1996) were used. It appears that these models do not cover the full range of age that might be necessary, and also that they badly disagree on some points, as already emphasized by the specialists (Charlot et al. 1996). For a given galaxy, a model is thus defined by the "old object" and an SSP. The old object population indices are those appropriate for *Nop* galaxies of the same $\log \sigma_0$. The SSP is defined by age, metallicity and its fractional contribution k_V to the V luminosity. The changes of population indices due to the SSP contribution remain small enough to be nearly proportional to k_V, or to the mass increment.

In Table 9 are intercompared the *observed and calculated* residual indices of two prototypical objects. For NG2865 are introduced 3 models, using SSP's by Bressan et al. (loc. cit.), of sub-solar metallicity (Z = 0.008), and 3 different choices of the age, i.e. 1, 0.75 and 0.5 Gyr. The k_V are roughly adjusted to obtain approximate agreement of the $\Delta B - V$ residual. For this object, the O−C are rather satisfactory, chiefly for the lower age values, except perhaps in $\Delta U - B$ or $\Delta B - R$, and surely in $\Delta V - I$ and $\Delta Mg b$. The smaller age cannot be fully tested due to lack of calculated indices. The agreement is less good with SSP's of larger metallicity (not tabulated). For NGC 3923, with its reddish residual indices, we offer models with 2 SSP's of the same age of 3 Gyr, a metallicity above solar ([Fe/H] = 0.4) and k_V = 0.3, but taken respectively from Bressan et al. and Worthey. The $V - R$ and $V - I$ metallicity gradients seem too large in Bressan et al. at above-solar Z-values. This may be the case for $B - V$ in Worthey, in agreement with this author comments.

The results of these numerical experiments are rather disappointing, because it does not seem generally feasible to reproduce the *relative values* of residual population indices: the calculated $U - B$ residuals are often too large (in absolute value) as compared to the $B - V$ ones, contrary to the empirical results displayed in Figs. 6 and 8, or Tables 6 and 7, while the reverse is true for the $B - R$ and $V - I$ colours. The basic model of a late event of star formation or capture, imposed upon a standard elliptical, remains however promising: it might explain both the blueish and reddish galaxies, *YP* and *NP*, encountered in the present survey.

Further work is planned, hopefully using more recent and extensive calculations of stellar populations, in the full relevant ranges of ages and metallicity.

One should finally note that, in view of the many different situations expected in relatively recent interactions of ellipticals with their neighbours, the detailed study of individual cases should be attempted, involving new and improved observations of populations parameters, and hopefully the consideration of dynamical scenarios for the event, including the possible role of nearby objects. A step in this direction is taken by Hau et al. (1999), who try to interpret the changes in 3 population indices, between the "bulge" of NGC 2865 and a spectroscopically apparent feature at the center of the object: their material is not yet sufficient however, to reach unambiguous conclusions.

Acknowledgements. Drs. T. Idiart and J. de Freitas Pacheco obtained a large part of the here used OHP frames. Most of the used frames were secured from the DSS.

– Northern part based on photographic data of the National Geographic Society – Palomar Observatory Sky Survey (NGS-POSS) obtained using the Oschin Telescope on Palomar Mountain. The NGS-POSS was funded by a grant from the National Geographic Society to the California Institute of

Technology. The plates were processed into the present compressed digital form with their permission. The Digitized Sky Survey was produced at the Space Telescope Science Institute under US Government grant NAG W-2166.

– Southern part based on photographic data obtained using The UK Schmidt Telescope. The UK Schmidt Telescope was operated by the Royal Observatory Edinburgh, with funding from the UK Science and Engineering Research Council, until 1988 June, and thereafter by the Anglo-Australian Observatory. Original plate material is copyright (c) the Royal Observatory Edinburgh and the Anglo-Australian Observatory. The plates were processed into the present compressed digital form with their permission.

References

Arp, H. 1966, Atlas of peculiar Galaxies, CALTECH, Pasadena
Barnes, J. R. 1988, ApJ, 331, 699
Barnes, J. R., & Hernquist, L. 1992, ARA&A, 30, 705
Bender, R., & Möllenhof, C. 1987, A&A, 177, 71
Bender, R. 1988, A&A, 193, L7
Bettoni, D. 1992, A&AS, 96, 333
Bressan, A., Chiosi, C., & Fagotto, F. 1994, ApJS, 94, 63
Bressan, A., Chiosi, C., & Tantalo, R. 1996, A&A, 311, 425
Bueing, J., Bender, R., Mendes de Oliveira, C., et al. 2002, A&A, 395, 431
Caon, N., Capaccioli, M., & D'Onofrio, M. 1994, A&AS, 106, 199
Carter, D. 1978, MNRAS, 182, 797
Carter, D., Prieur, J. L., Wilkinson, A., et al. 1988, MNRAS, 235, 813
Charlot, S., Worthey, G., & Bressan, A. 1996, ApJ, 457, 625
Colbert, J. W., Mulchaey, J. S., & Zabludoff, A. I. 2001, AJ, 121, 808
Combes, F., Rampazzo, R., Bonfanti, P., et al. 1995, A&A, 297, 37
de Zeeuw, T., & Franx, M. 1991, ARA&A, 29, 239
Fort, B. P., Prieur, J. L., Carter, D., et al. 1986, ApJ, 306, 110
Giudicelli, M., & Michard, R. 1993, Proc. 5th ESO/ST-ECF Workshop
Goudfrooij, P., Hansen, L., Jørgensen, H. E., et al. 1994, A&AS, 104, 179
Hau, G. K. T., Carter, D., & Balcells, M. 1999, MNRAS, 306, 437
Higdon, J. L., Buta, R. J., & Purcell, G. B. 1998, AJ, 115, 80
Idiart, T., Michard, R., & de Freitas Pacheco, J. 2002, A&A, 383, 30
Kormendy, J., & Bender, R. 1996, ApJ, 464, L119
Kuntschner, H. 2000, MNRAS, 315, 184
Kuntschner, H., Lucey, J. R., Smith, R. J., et al. 2001, MNRAS, 323, 615
Kuntschner, H., Smith, R. J., Colless, M., et al. 2002, MNRAS, 337, 172
Lima-Neto, G. B., & Combes, F. 1995, A&A, 294, 657
Michard, R. 1985, A&AS, 59, 205
Michard, R. 1994, A&A, 288, 401
Michard, R. 1999, A&AS, 137, 245
Michard, R. 2002, A&A, 384, 763
Michard, R., & Marchal, J. 1994, A&AS, 105, 481
Malin, D. F. 1979, Nature, 277, 279
Malin, D. F., Carter, D. 1983, ApJ, 274, 534 (MC83)
Malin, D. F., & Hadley, B. 1999, in Galaxy Dynamics, ed. D. Merritt, J. A. Sellwood, & M. Valluri, ASP Conf. Ser., 182
Oosterlo, T., Balcells, M., & Carter, D. 1994, MNRAS, 266, L10
Poulain, P., & Nieto, J.-L. 1994, A&AS, 103, 573
Prieur, J. L. 1988a, ApJ, 326, 596
Prieur, J. L. 1988b, Ph.D. Thesis, Univ. Paul Sabatier, Toulouse
Prugniel, P., Nieto, J. L., Bender, R., et al. 1988, A&A, 204, 61
Prugniel, P., & Simien, F. 1996, A&A, 309, 749 (PS96)
Prugniel, P., & Simien, F. 1997, A&A, 321, 111
Prugniel, P., & Héraudeau, P. 1998, A&AS, 128, 299
Prugniel, P., Golev, V., & Maubon, G. 1999, A&A, 346, L25
Sansom, A. E., Reid, I. N., & Boisson, C., MNRAS, 234, 247
Schweizer, F., & Ford, W. K. 1985, in New Aspects of Galaxy Photometry, Proc. 8th IAU Regional European Meet., Toulouse 1984, ed. J. L. Nieto (Springer Verl.)
Schweizer, F., & Seitzer, P. 1988, ApJ, 328, 88
Schweizer, F., Seitzer, P., Faber, S. M., et al. 1990, ApJ, 364, L33
Schweizer, F., & Seitzer, P. 1992, AJ, 104, 1039 (SS92)
Scorza, C., & Bender, R. 1995, A&A, 293, 20
Scorza, C., Bender, R., Winkelmann, C., et al. 1998, A&AS, 131, 265
Tonry, J. L., Dressler, A., Blakeslee, J. P., et al. 2001, ApJ, 546, 681
Toomre, A., & Toomre, J. 1972, ApJ, 178, 623
Toomre, A. 1977 in The Evolution of Galaxies and Stellar Populations, ed. B. Tinsley, & R. Larson (Yale Univ. Obs. New Haven.)
Trager, S. C., Worthey, G., Faber, S. M., et al. 1998, ApJS, 116, 1
Trager, S. C., Faber, S. M., Worthey, G., et al. 2000, AJ, 119, 1645
Wernli, F., Emsellem, E., & Copin, Y. 2001, in SF2A Scient. Highl., ed. F. Combes et al. (Les Ulis: EDP Sciences)
Worthey, G. 1994, ApJS, 95, 107

Online Material

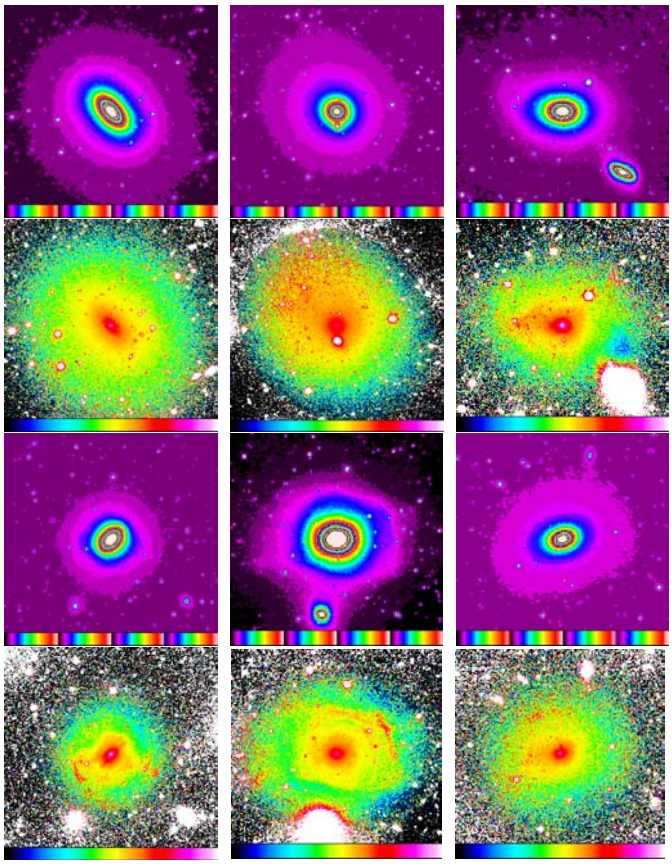

Fig. 1. Displays of the direct and masked images of 6 ellipticals from OHP observations. 1st row from top, left to right: direct images of NGC 3377, field 7.9′; NGC 5846, 9.2′; NGC 5576, 6.8′. 2nd row: masked images of the same objects. 3rd row, left to right: direct images of NGC 3610, 6.8′; NGC 3640, 6.8′; NGC 5982, 6.8′. 4th row: masked images of the same objects.

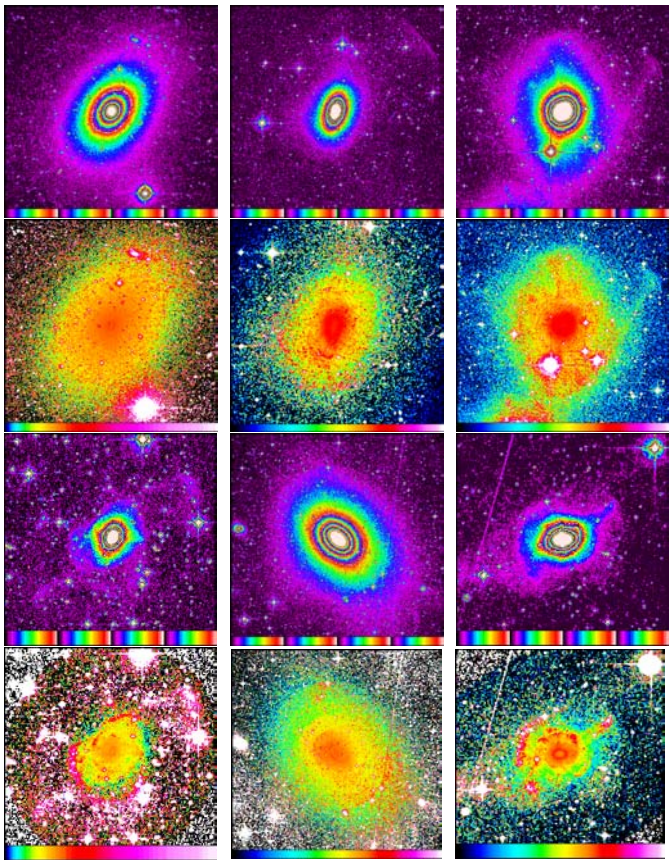

Fig. 2. Displays of the direct and masked images of 6 ellipticals from DSS frames. 1st row from top, left to right: direct images of NGC 4636, field 17′; NGC 1344, 17′; NGC 1549 17′. 2nd row: masked images of the same objects (field only 10′ for NGC 1344). 3rd row, left to right: direct images of NGC 2865, 10′; NGC 3923, 17′; NGC 5018, 10′. 4th row: masked images of the same objects.

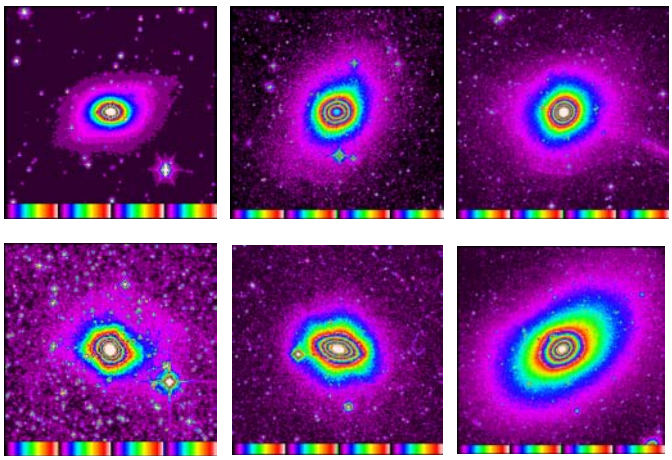

Fig. 3. Displays of the direct images of 6 ellipticals. Upper row, left to right: NGC 1700 (OHP CCD frames) field 6.8′; NGC 1395, 17′, NGC 4552, 17′. Lower row: IC 3370, 10′, NGC 4125, 17′; NGC 4406, 17′ (all 5 from the DSS).